doi:10.1093/brain/awv166 BRAIN 2015: 138; 2383–2398 | 2383

BRAIN
A JOURNAL OF NEUROLOGY

# CYP46A1 inhibition, brain cholesterol accumulation and neurodegeneration pave the way for Alzheimer's disease

**Fathia Djelti,[1] Jerome Braudeau,[1,*] Eloise Hudry,[1,*] Marc Dhenain,[2] Jennifer Varin,[3] Ivan Bièche,[3] Catherine Marquer,[4] Farah Chali,[4] Sophie Ayciriex,[5] Nicolas Auzeil,[5] Sandro Alves,[1] Dominique Langui,[4] Marie-Claude Potier,[4] Olivier Laprevote,[5] Michel Vidaud,[3] Charles Duyckaerts,[4] Richard Miles,[4] Patrick Aubourg[1,*] and Nathalie Cartier[1,*]**

*These authors contributed equally to this work.

Abnormalities in neuronal cholesterol homeostasis have been suspected or observed in several neurodegenerative disorders including Alzheimer's disease, Parkinson's disease and Huntington's disease. However, it has not been demonstrated whether an increased abundance of cholesterol in neurons *in vivo* contributes to neurodegeneration. To address this issue, we used RNA interference methodology to inhibit the expression of cholesterol 24-hydroxylase, encoded by the *Cyp46a1* gene, in the hippocampus of normal mice. Cholesterol 24-hydroxylase controls cholesterol efflux from the brain and thereby plays a major role in regulating brain cholesterol homeostasis. We used an adeno-associated virus vector encoding short hairpin RNA directed against the mouse *Cyp46a1* mRNA to decrease the expression of the *Cyp46a1* gene in hippocampal neurons of normal mice. This increased the cholesterol concentration in neurons, followed by cognitive deficits and hippocampal atrophy due to apoptotic neuronal death. Prior to neuronal death, the recruitment of the amyloid protein precursor to lipid rafts was enhanced leading to the production of β-C-terminal fragment and amyloid-β peptides. Abnormal phosphorylation of tau and endoplasmic reticulum stress were also observed. In the APP23 mouse model of Alzheimer's disease, the abundance of amyloid-β peptides increased following inhibition of *Cyp46a1* expression, and neuronal death was more widespread than in normal mice. Altogether, these results suggest that increased amounts of neuronal cholesterol within the brain may contribute to inducing and/or aggravating Alzheimer's disease.

1 INSERM U1169 Le Kremlin-Bicêtre and Université Paris-Sud, 91400 Orsay, France
2 CNRS URA2210 MIRCen CEA Fontenay aux Roses 92265, and Université Paris-Sud, 91400 Orsay, France
3 EA7331, Université Paris Descartes Sorbonne Paris Cité, Faculté des Sciences Pharmaceutiques et Biologiques, 75006 Paris, France
4 UMR S1127, and INSERM U1127, and CNRS UMR7225, and ICM, Sorbonne Université, UPMC Univ Paris 06 75013, Paris, France
5 Chimie-Toxicologie Analytique et Cellulaire, EA 4463, Université Paris Descartes, Sorbonne Paris Cité, Faculté des Sciences Pharmaceutiques et Biologiques, 75006 Paris, France

Correspondence to: Nathalie Cartier,
INSERM U1169,
Le Kremlin-Bicêtre and Université Paris-Sud,
91400 Orsay,
France
E-mail: nathalie.cartier@inserm.fr

Received November 4, 2014. Revised April 15, 2015. Accepted April 17, 2015. Advance Access publication July 3, 2015

**Keywords:** cholesterol; 24S-hydroxycholesterol; *Cyp46a1*; Alzheimer's disease; neurodegeneration

**Abbreviations:** AAV = adeno-associated virus; β-CTF = beta C-terminal fragment; CHOP = C/EBP-homologous protein; GSK3β = glycogen synthase kinase 3-beta; PERK = protein kinase RNA (PKR)-like endoplasmic reticulum kinase

# Introduction

There is a growing body of evidence of a strong association between abnormalities in brain cholesterol homeostasis (especially high concentrations in neurons) and several neurodegenerative disorders, including Alzheimer's disease, Huntington's disease and Parkinson's disease (Vance, 2012). However, there has been no experimental demonstration that increased cholesterol concentrations in neurons may result in neurodegeneration *in vivo*. We therefore used an RNA interference strategy to downregulate cholesterol 24-hydroxylase activity in mouse hippocampal neurons. Cholesterol 24-hydroxylase plays a major role in regulating cholesterol homeostasis within the adult brain (Dietschy and Turley, 2004).

Cholesterol does not freely cross the intact blood–brain barrier and nearly all cholesterol in the adult brain is synthesized *in situ* by astrocytes (Dietschy and Turley, 2001). Only 0.02% of the cholesterol in the adult brain undergoes a turnover each day and thus most is metabolically inert (Dietschy and Turley, 2004). The cholesterol abundance in the CNS depends primarily on local synthesis and efflux (Dietschy and Turley, 2004; Bjorkhem, 2006). However, cholesterol cannot be exported directly from the brain. It is converted to 24S-hydroxycholesterol by cholesterol 24-hydroxylase (encoded by the *CYP46A1* gene), a highly conserved cytochrome P450 enzyme, which can be exported across the blood–brain barrier and is metabolized into bile acids in the liver (Bjorkhem *et al.*, 1998; Russell *et al.*, 2009). The levels of 24S-hydroxycholesterol in the circulation are high during the first months of life, while there is a rapid expansion of the cholesterol pool in the brain (Lutjohann *et al.*, 2001). Subsequently, the levels of 24S-hydroxycholesterol are extremely stable in adulthood (Lutjohann *et al.*, 1996). At the age of 1 year in humans (2–4 weeks in mice), the expression of cholesterol 24-hydroxylase reaches a steady state which is maintained during adulthood (Lund *et al.*, 1999). In normal human adult brain, cerebral cholesterol 24-hydroxylase is mostly expressed in pyramidal cells of the cortex and hippocampus, granule cells of the dentate gyrus, purkinje cells of the cerebellum and neurons of the thalamus (Lund *et al.*, 1999). Cholesterol 24-hydroxylase activity is abnormal in the brain of patients with Alzheimer's disease (Bogdanovic *et al.*, 2001).

In transgenic lines where *Cyp46a1* is overexpressed or is inactivated by knockout, cholesterol levels remain the same as in the wild-type due to up- or downregulation, respectively, of cholesterol synthesis (Lund *et al.*, 2003; Xie *et al.*, 2003; Shafaati *et al.*, 2011). This shows that alterations of *Cyp46a1* expression at an early developmental stage are compensated by homeostatic adaptation of cholesterol metabolism, and in particular cholesterol synthesis. To increase neuronal cholesterol *in vivo* experimentally, we used an adeno-associated virus (AAV) carrying a short hairpin (sh) directed against *Cyp46a1* RNA (shCYP46A1) in the hippocampus of adult mice.

Herein, we show that decreased *Cyp46a1* gene expression in the hippocampus of normal mice results in increased amounts of cholesterol in neurons. This cholesterol accumulation leads to apoptotic death of neurons and thereby cognitive impairments. Downregulation of *Cyp46a1* expression also leads to the production of amyloid-β peptides and the abnormal phosphorylation of tau protein. In APP23 mice, a model of Alzheimer's disease, the consequences of *Cyp46a1* downregulation are more pronounced. These various findings demonstrate that cholesterol accumulation sensitizes neurons to Alzheimer's disease-like pathology.

# Materials and methods

## Animals and intracerebral injection of AAV vectors

Three-month-old female wild-type C57Bl/6 and 5-month-old APP23 transgenic mice (Thy1-hAPPswe) were used (average weight 20–25 g). The mouse line APP23 was generously provided by Mathias Staufenbiel (Novartis Pharma). These mice overexpress the mutated human $APP_{751}$ gene containing the Swedish double mutation (K670N-M671L) under the control of the neuron-specific promoter *Thy1*. Animals were housed in pathogen-free conditions under a 12-h light-dark cycle. Experiments were approved by the Animals Ethics Committee of INSERM. This work was performed in accordance with the Directive 86/89/EEC of the European Committee Council, and INSERM and local guidelines.

Mice were anaesthetized by intraperitoneal injection of ketamine (80 mg/kg) and xylazine (50 mg/kg) and placed in a stereotaxic frame (D Kopf Instruments). Stocks of the AAV5 vectors encoding scramble or shCYP46A1 sequences were generated by transient transfection of 293T cells and purified on caesium chloride ultracentrifugation gradients (Sevin *et al.*, 2006) (Supplementary Table 1). Titres ranged from 4 to $9 \times 10^{12}$ vector genomes (vg)/ml. Two microlitres of phosphate-buffered saline solution (PBS1X) or of viral vector (corresponding to $2 \times 10^9$ vg) was injected into the left and right hippocampi with a 10 µl Hamilton syringe attached to a 30-gauge needle at a rate of 0.2 µl/min. The coordinates of the injection sites were: anterior-posterior 2 mm, medial-lateral ± 1.2 mm, dorsal-ventral −2 mm, with respect to the bregma.

In each experiment, one group of mice was injected with the AAV-scramble vector and one with the AAV-shCYP46A1

vector. C57BL/6 mice were sacrificed 2, 3, 4, 6, 8 and 12 weeks after injection for immunohistochemical and biochemical studies. APP23 mice were sacrificed at 4 weeks after injection (Supplementary Table 2).

## Gene expression analysis by quantitative reverse transcription PCR and western blot

Anaesthetized animals were transcardially perfused with PBS1X. The hippocampus of each injected hemisphere was dissected out, snap-frozen in liquid nitrogen and ground in liquid nitrogen with a mortar and pestle.

All biochemical measures used the right hemisphere and results are reported in arbitrary units. Half the ground tissue was used to isolate total RNA with the RNAble kit (Eurobio laboratories). Quantitative RT-PCR analysis was performed using the ABI Prism 7900 sequence detection system (Perkin-Elmer) as described previously (Bieche *et al.*, 2004). Transcripts of the TATA-box binding protein gene (*Tbp*) were used as an endogenous RNA control. Primers for *Tbp* and the other genes were designed with Oligo 5.0 software (National Biosciences, Supplementary Table 3). Target transcript levels (N-target) were normalized to the *Tbp* transcript levels and mRNA level with the equation N-target = 2.$\delta$Ct where $\delta$Ct is the Ct value of the target gene after subtraction of Ct for the *Tbp* gene. Gene expression in AAV-scramble injected hippocampus did not change significantly with time.

The other half of the tissue was used for the biochemical analyses. Total protein was extracted with Tris-buffered saline (TBS1X) containing 1% Triton™ X-100, a protease inhibitor cocktail (complete mini EDTA, Roche) and phosphatase inhibitor (Pierce). The total protein concentration was determined using the BCA Protein Assay Kit-Reducing Agent Compatible (Pierce). Lysates were stored at −80°C. For western blotting, proteins were resolved on precast polyacrylamide 4–12% gels (precast Criterion™, BIS-Tris, Bio-Rad) in buffer (NuPAGE®, Life Technologies), then transferred onto nitrocellulose membranes. The membranes were blocked in TBS1X containing 5% non-fat milk powder and 0.1% Tween-20 for 20 min at room temperature, then incubated overnight at 4°C with antibodies against cholesterol-24-hydroxylase (1:1000, Millipore), APP (1:750, Calbiochem) or flotillin 1 (1:1000, BD biosciences). Blots were then incubated with horseradish peroxidase-IgG conjugates (GE Healthcare), and signals were revealed with a chemiluminescence kit (GE Healthcare) and quantified by densitometry analysis of scanned autoradiograms (ImageJ, ver 1.38, NIH).

## Determination of cholesterol and 24S-hydroxycholesterol contents in hippocampus

Cholesterol was assayed in lipids extracted from hippocampus protein lysates (see above) by treatment with a solution containing chloroform and methanol (2:1) and centrifugation at 13 000 rpm. The organic phase was recovered, and chloroform and methanol were removed by vacuum extraction. The dried lipids were dissolved in isopropanol containing 10% Triton™ X-100. Cholesterol was quantified fluorometrically (Amplex Red Cholesterol assay kit, Life Technologies) according to the manufacturer's instructions. Briefly, 2 µl samples of the lipid extract were added to a reaction mix including Amplex® Red, horseradish peroxidase, cholesterol oxidase and cholesterol esterase. After 30 min at 37°C, fluorescence was measured (microplate reader, FLUOstar Optima, BMG LabTek) by excitation at 550 nm and detection at 590 nm.

For 24S-hydroxycholesterol measurements, weighed hippocampus tissues were homogenized in cold water containing butylated hydroxyl toluene (0.1%) with a Precellys®24-Dual (Precellys) tissue homogenizer for 15 s at 5000 rpm. Five microlitre aliquots of homogenate were used for protein assays (Bradford assay). Lipids were extracted with a hexane and methanol mixture (3:1 v/v) by mechanical shaking for 1 h at room temperature. Extracts were centrifuged at 2500 rpm for 10 min to separate the phases. The organic (upper) phase was collected and washed with water (600 µl) for 10 min with mechanical agitation. The phases were separated, and the upper phase was collected and resuspended in dichloromethane and spiked with 24(R/S)-hydroxycholesterol (d6) (20 ng) as a standard for oxysterols (Avanti Polar Lipids). Oxysterols were derived and analysed by ultra-performance liquid chromatography coupled to high-resolution mass spectrometry, as described (Ayciriex *et al.*, 2012). The content in AAV-shCYP46A1 samples was normalized to that in AAV-scramble samples.

## Determination of amyloid-$\beta_{40}$, amyloid-$\beta_{42}$, β-CTF and phosphorylated forms of tau concentrations

Amyloid-$\beta_{40}$, amyloid-$\beta_{42}$, β-C-terminal fragment (β-CTF) and phosphorylated-tau (Thr181) were assayed in hippocampal lysate (aliquots containing 3 mg of protein) using INNOTEST® β-amyloid 1–40 (Innogenetics), INNOTEST® β-amyloid 1–42 APP β-CTF (IBL) and INNOTEST® phospho-tau Thr181 (Innogenetics) ELISA kits, respectively. ELISA kits were used following supplier instructions and results are expressed in ng or pg per mg of protein.

## Isolation of hippocampal rafts

Three hippocampi were pooled and lysed in TBS1X containing 1% Triton™ X-100, a protease inhibitor cocktail (complete mini EDTA, Roche) and phosphatase inhibitor (Pierce). All steps were performed at 4°C. The protein concentration was adjusted to 3 mg/ml and sucrose was added to 40%. Layers of 35% and 5% sucrose, both in TBS buffer, were overlaid in an ultracentrifuge tube. After ultracentrifugation at 34 200 rpm for 18 h at 4°C, fractions of 1 ml were collected from the top (Fraction 1) to the bottom of the gradient. Fractions were analysed by standard western blotting protocols. The detergent-resistant membrane (DRM) fractions were enriched in flotillin 1 protein.

## Immunohistochemical analysis

Brain tissues were obtained 2, 3, 4, 6, 8 and 12 weeks following injection of AAV-scramble or AAV-shCYP46A1 vectors ($n = 5$ mice for each time point and vector). Animals were lethally anaesthetized and intracardially perfused with PBS1X

(Life Technologies). Tissue samples were collected and post-fixed in 4% paraformaldehyde for 24 h at 4°C, then embedded in paraffin. Sections 6-µm thick were cut, deparaffinized in xylene and rehydrated in ethanol. For several antibodies, an antigen retrieval step in citric acid (0.1 mol/l)/sodium citrate (0.1 mol/l) buffer was necessary. Sections were permeabilized in PBS1X/0.1% Triton for 10 min at room temperature, blocked in PBS1X/0.1% Triton/5% normal goat serum for 30 min at room temperature, then incubated overnight at 4°C with primary antibody: anti-GFP coupled to biotin (1:200, Abcys), anti-GFAP coupled to Cyanine 3 (1:200, Sigma Aldrich), polyclonal anti-IBA1 (1:200, Wako), anti-NeuN coupled to biotin (1:200, Millipore), polyclonal anti-Znt3 (1:200, kindly provided by R. Palmiter, University of Washington), polyclonal anti-Rab5 (1:250, Santa Cruz), polyclonal anti-GSK3β monoclonal anti p-tau mouse (AT180, p-Thr231/Ser235, 1:200, Pierce), polyclonal anti-CHOP (1:500; Novus biological), polyclonal anti p-PERK (Thr981, 1/400, Santa-Cruz) polyclonal anti-cleaved caspase 9 (1:200, Cell Signaling Technology), polyclonal anti-cleaved caspase 3 (1:200, Cell Signaling Technology) polyclonal anti-caspase 12 (1:500, Cell Signaling Technology, which recognizes the inactive and active forms of caspase 12). Secondary antibodies were applied for 1 h at room temperature. Slides were then mounted in VECTASHIELD® mounting medium containing DAPI (Vector Laboratories) and examined by fluorescence or confocal microscopy. Fluorescence images were taken with a Nikon microscope (Eclipse 800) and a digital QImaging camera (CCD QICAM cooled plus RGB filter pixel 4.65 × 4.65 µm). For confocal microscopy, we used a Zeiss LSM 710 confocal microscope (CarlZeiss) with a Plan Apochromat 63/1.4 NA oil-immersion objective using the LSM510v4.0sp2 or Zen 2009 (Carl Zeiss).

AAV-scramble and AAV-shCYP46A1 slices were processed on the same day, in parallel under the same conditions. Neuronal density in the CA1, CA3a and CA3b regions was estimated from three consecutive hippocampal sections from mice killed 2, 3, 4, 6, 8 and 12 weeks after injection using HistoLab image analyser software ($n = 5$ mice per vector per time, sections at three levels per mouse) (Microvision Instrument France). The mean NeuN-positive cell counts were compared to the number of NeuN-positive cells in hippocampi from AAV-scramble-injected mice. The number of NeuN-positive cells in AAV-scramble-injected hippocampi did not change significantly with time.

Percentages of CA3a pyramidal neurons showing immunostaining for phosphorylated (p)-tau, p-GSK3β, p-PERK (Thr981), CHOP, cleaved caspase 9 and cleaved caspase 3, were evaluated using HistoLab image analyser software (Microvision Instrument France) ($n = 5$ mice per vector per time, three sections per mouse). The intensity of GFP and caspase 12 labelling was evaluated in 60 pyramidal cells per mouse ($n = 5$ mice per vector, six sections) with ImageJ software.

The number and the size of RAB5-positive endosomes were measured in 60 CA3a pyramidal cells per mouse ($n = 5$ mice per vector, six sections) with ImageJ software.

For filipin staining, serial sections (50-µm thick) were cut with a vibratome, cryoprotected in 30% sucrose and 30% ethylene glycol in phosphate buffer and kept at −20°C. Slices were fixed with 4% paraformaldehyde, washed and exposed to 50 µg/ml filipin in phosphate buffer for 2 h in complete darkness, without permeabilization of cell membranes. Samples were immediately examined with an SP5 confocal microscope (Leica Microsystems) with UV laser excitation at 351 nm. Emitted light between 400 and 680 nm was detected with a ×60 oil-immersion objective (Nikon). Filipin imaging was performed at the CPBM/ CLUPS/ LUMAT FR2764 imaging facility (Université Paris-Sud, Orsay).

## Electron microscopy

C57Bl/6 mice were perfused with 4% paraformaldehyde and 2.5% glutaraldehyde in phosphate buffer 0.1 M pH 7.4. Brains were removed and post-fixed in 2.5% glutaraldehyde in phosphate buffer 0.1 M, pH 7.4. The fluorescent region of the hippocampus of C57Bl/6 mice injected with AAV-scramble or AAV-shCYP46A1 was excised under a fluorescence binocular dissecting microscope (Leica). Sections (50-µm thick) were cut with a vibratome and post-fixed in 1% osmium tetroxide for 30 min, rinsed in phosphate buffer, dehydrated in a graded series of ethanol solutions (75, 80, 90 and 100%), infiltrated with Epon™ 812 and placed in moulds. The resin was cured at 60°C in a dry oven for 48 h. Semi-thin sections (0.5-µm thick) of the hippocampus preparations were cut with a Leica UC7 ultramicrotome. Ultrathin (90 nm) sections were cut and counterstained with uranyl acetate and lead citrate. They were examined with a Hitachi HT7700 electron microscope, operating at 80 kV. Pictures (2048 × 2048 pixels) were taken with an AMT41B (pixel size 7.4 µm × 7.4 µm).

## Behaviour

All behavioural studies were performed 8 weeks after vector injection.

### Open-field

The apparatus consisted of an open-topped arena measuring 50 × 50 × 38 cm consisting of a central region (10 × 10 cm) and a peripheral region, placed in a room with defined, weak luminosity (25 lx). Mice were placed in the centre of the arena and behaviour was analysed for 20 min from video files: the times spent in the centre and in the periphery of the open-field were measured. Data were collected using Ethovision 9.0 software (Noldus Information Technology, Wageningen, The Netherlands). The periphery/centre ratio was calculated and served as an emotional behaviour index.

### Exploratory activity

Environment exploration was assessed by monitoring mice over a 24-h period. In the experimental room, mice were placed in a cage with food and water available (30.5 cm × 30.5 cm × 43.5 cm; Noldus Information Technology). They were observed during both light and dark phases with a closed circuit television camera and an infra-red lamp. Tracking was performed using Ethovision 8.5 software (Noldus Information Technology, Wageningen, The Netherlands) that recorded horizontal movements throughout the 24-h period.

### Morris water maze

A 120-cm diameter Morris water maze filled with opaque water at 20–21°C with a 9-cm diameter platform submerged 1.0 cm under the water surface was used.

Mice were trained for six consecutive days ($n = 10$ mice per group). Training consisted of daily sessions (three trials per session). Start positions varied pseudorandomly among the four cardinal points. The mean intertrial interval was 1 h.

During the spatial training phase, each trial ended when the animal reached the platform. If the mice did not find the platform in 60 s (cut-off time), they were manually guided to the platform. Once on the platform, animals were allowed to rest for 30 s and then returned to their home cage. The distance travelled to reach the platform was evaluated for every trial. Four hours after the last training trial, spatial retention was assessed using a probe trial in which the platform was no longer available. For the probe trial, the percentages of the total time in target and other quadrants were determined. Data were collected using Ethovision 9.0 software (Noldus Information Technology, Wageningen, The Netherlands).

## MRI acquisition and processing

A 7 T spectrometer (Agilent) interfaced with a console running VnmrJ 2.3 was used to record images of the *in vivo* brain, 12 weeks after injection. The spectrometer was equipped with a rodent gradient insert of 700 mT/m. A birdcage coil (RapidBiomed) and a mouse brain surface coil (RapidBiomed) actively decoupled from the transmitting birdcage probe were used for emission and reception, respectively. Animals were anaesthetized with isofluorane (5% for induction, 1–2% for maintenance). The respiration rate was monitored during image acquisition. Two-dimensional fast spin-echo images were recorded with an in-plane resolution of $78 \times 78\,\mu m^2$ zero-filled to $39 \times 39\,\mu m^2$ (repetition time/echo time/effective-echo time = 6000/12/36 ms, echo train length = 4, number of averages = 4, field of view = 2 × 2 cm, matrix = 256 × 256, reconstructed matrix = 512 × 512, 64 successive slices, slice thickness = 200 µm).

Volumes were measured with Anatomist® software (http://brainvisa.info/index_f.html). Before morphometric analysis, the brain images were rotated so that those for all mice were in a similar orientation. The hippocampi were manually outlined on 10 successive coronal sections with a digitizing tablet (Anatomist drawing tools). Coronal sections spanned the range −0.94 mm to −3.52 mm from Bregma. The intracranial volume of the 10 sections was outlined and measured, and volumes of hippocampal regions were corrected for the total brain volume.

## Statistical analysis

Statistical analyses involved two-tailed unpaired *t*-tests. Some data were analysed with one-way (with Newman-Keuls *post hoc*) or two-way (with Bonferroni's *post hoc*) comparison analyses of variance (ANOVA). ANOVA with repeated measures were carried out as appropriate to assess complementary statistical effects. A *P*-value $<0.05$ was considered to indicate statistical significance. Analyses were performed using Statistica v6 (StatSoft Inc.) or GraphPad Prism (GraphPad Software) software.

# Results

## Inhibition of *Cyp46a1* expression in the hippocampus decreases 24S-hydroxycholesterol and increases neuronal cholesterol content

Eleven small hairpin RNA (shRNA) sequences directed against *Cyp46a1* mRNA were designed with the Promega algorithm. In parallel, a scramble sequence, which had no similarity to endogenous mRNA, was used as a negative control (Supplementary Table 1). We selected the shRNA sequence best able to inhibit *Cyp46a1* expression *in vitro* and *in vivo* (Supplementary material and Supplementary Fig. 1).

AAV vectors encoding the shRNA selected for interfering with *Cyp46a1* expression (shCYP46A1) or the scramble sequence and enhanced green fluorescent protein (GFP) were injected bilaterally into the dorsal hippocampus (stratum lacunosum moleculare) of C57Bl/6 mice (Fig. 1A).

Two weeks after injection into normal mice, enhanced GFP was detected in pyramidal cells of the CA3 and to a lesser extent of the CA1 regions (Fig. 1A and Supplementary Fig. 2A). The dorsal hippocampus is crossed by perforant path fibres that innervate CA3a and CA1 pyramidal cells (Ishizuka *et al.*, 1995). Co-immunostaining with an antibody against Znt3 (encoded by *Slc30a3*), a mossy fibre marker (Palmiter *et al.*, 1996), showed that enhanced GFP-positive cells were mostly in the CA3a region (Fig. 1B). Expression of enhanced GFP was restricted to neurons (Fig. 1B) and remained stable up to 12 weeks after injection. There was no difference between the enhanced GFP expression profiles following injection of the AAV-scramble vector and those following injection of the AAV-shCYP46A1 vector (Supplementary Fig. 2A and data not shown).

We found no evidence that this RNA interference strategy induced off-target effects, such as activation of the innate immune response (Bauer *et al.*, 2009) (Supplementary Fig. 2B) or saturation of miRNA processing machinery (Grimm *et al.*, 2006) (Supplementary Fig. 2C). Injection of the AAV-shCYP46A1 vector rapidly and robustly inhibited the hippocampal expression of *Cyp46a1* (Fig. 1C) and of the cholesterol-24-hydroxylase protein (Fig. 1D). *Cyp46a1* gene expression was reduced by $52.5 \pm 5\%$ 2 weeks after injection, and by $81 \pm 4.6\%$ after 6 weeks (Fig. 1C). The level of cholesterol-24-hydroxylase protein was reduced by $39.7 \pm 0.3\%$ after 2 weeks and $92 \pm 1.5\%$ after 6 weeks (Fig. 1D). *Cyp46a1* gene and protein expression were unchanged in animals injected with the AAV-scramble control vector or with phosphate-buffered saline solution (data not shown).

Inhibition of *Cyp46a1* gene expression led to a decrease of the 24S-hydroxycholesterol content in hippocampus,

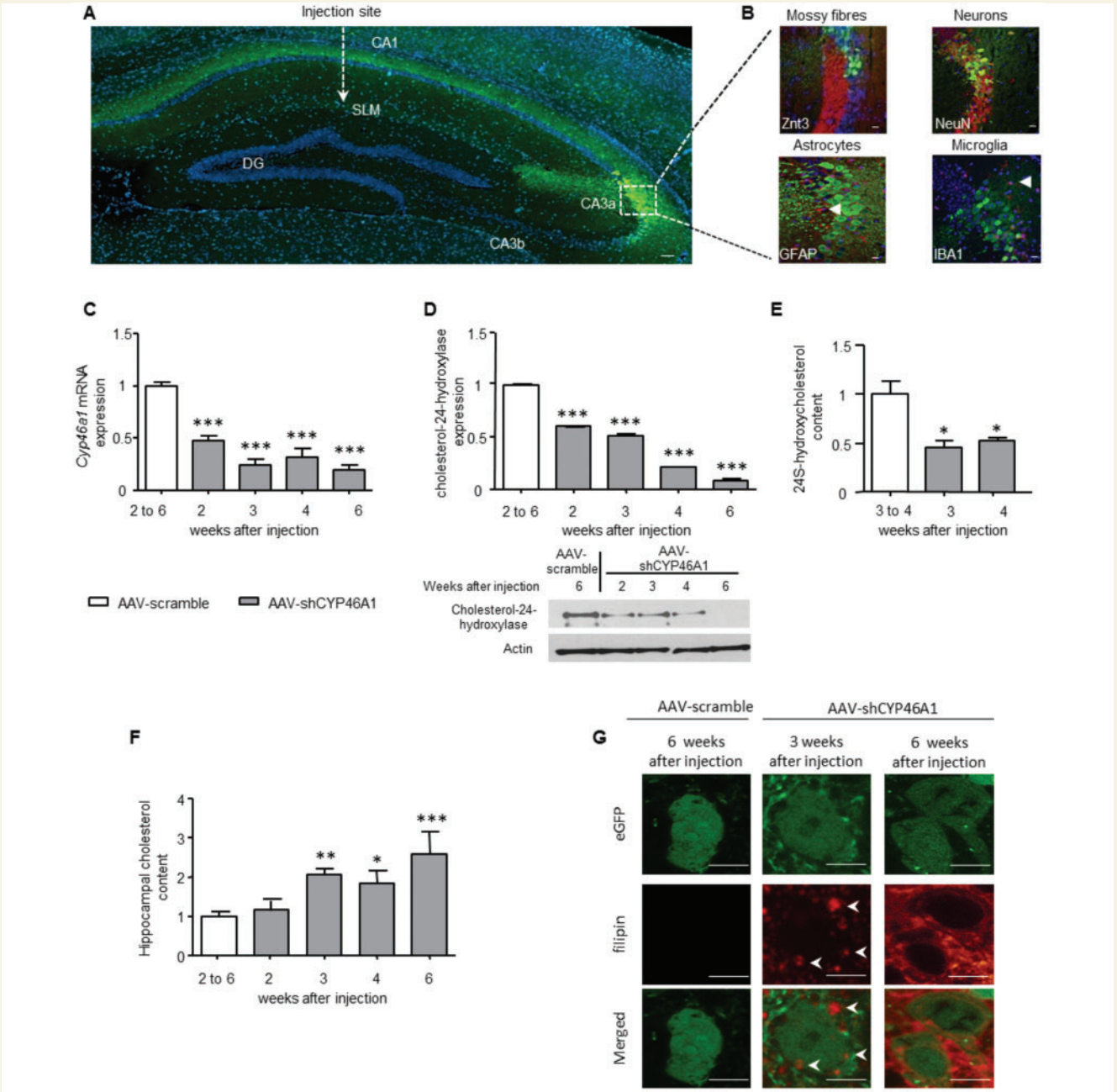


**Figure 1 Hippocampal injection of AAV-shCYP46A1 leads to downregulation of cholesterol-24 hydroxylase activity and an increased cholesterol content in neurons**. AAV vectors expressing enhanced GFP (eGFP) and shCYP46A1 or a scramble sequence were injected into the hippocampal stratum lacunosum moleculare of 3-month-old normal mice. (**A**) Enhanced GFP immunostaining (green) of AAV-shCYP46A1-injected hippocampus 3 weeks after injection. SLM = stratum lacunosum moleculare; CA = cornu ammonis; DG = dentate gyrus. Scale bar = 100 μm. (**B**) Double immunolabelling for enhanced GFP immunoreactivity (green) and Znt3 (mossy fibre marker, red), NeuN (neuronal marker, red), GFAP (astroglial marker, red) or IBA1 (microglial cell marker, red) in the CA3a region of AAV-shCYP46A1-injected mice 3 weeks after injection. Scale bar = 50 μm. (**C**) Quantitative hippocampal expression of murine *Cyp46a1* gene 2 to 6 weeks after injecting AAV-scramble or AAV-shCYP46A1 vectors ($n = 5$ mice per time point and per vector). $^{***}P < 0.0001$ one-way ANOVA with Newman-Keuls *post hoc* test. (**D**) Cholesterol-24-hydroxylase protein quantified by western blotting in the hippocampus 2 to 6 weeks after injection of AAV-scramble or AAV-shCYP46A1 vector ($n = 5$ mice per time point and per vector). $^{***}P < 0.0001$ by one-way ANOVA with Newman-Keuls *post hoc* test. Representative western blot of hippocampal cholesterol-24-hydroxylase enzyme 2 to 6 weeks after injecting AAV-scramble or AAV-shCYP46A1 vectors. (**E**) 24S-hydroxycholesterol content in hippocampus 3 and 4 weeks after injecting AAV-scramble and AAV-shCYP46A1 vector (content normalized to that of AAV-scramble injected animals, $n = 5$ mice per time point and per vector). $^{*}P < 0.05$, one-way ANOVA with Newman-Keuls *post hoc* test. (**F**) Hippocampal cholesterol content at 2 to 6 weeks after injecting AAV-scramble or AAV-shCYP46A1 vector (content normalized to that of AAV-scramble injected mice, $n = 5$ mice per time point and per vector). $^{*}P < 0.05$, $^{**}P < 0.005$, $^{***}P < 0.0001$, one-way ANOVA with Newman-Keuls *post hoc* test. (**G**) Immunostaining for enhanced GFP (green) and filipin (red) in the hippocampal CA3a region of normal mice 3 and 6 weeks after injection of AAV-scramble or AAV-shCYP46A1 vector. Scale bar = 6 μm.

by 47.5 ± 5% at 3 weeks and 54.3 ± 8.4% at 4 weeks (Fig. 1E). The total hippocampal cholesterol content increased 2 to 2.5-fold (Fig. 1F). We used filipin, a fluorescent compound that binds to unesterified cholesterol (Cooper and McLaughlin, 1984), to study the cholesterol content at the cellular level. No staining was detected in enhanced GFP-positive CA3a pyramidal cells of mice injected with the AAV-scramble vector (Fig. 1G). In contrast, filipin inclusions were detected in enhanced GFP-positive CA3a cells 3 weeks after injecting the AAV-shCYP46A1 vector. Filipin staining increased with time and high intensity spots were present throughout the cytoplasm 6 weeks after injection (Fig. 1G). No filipin staining was detected in glial cells (data not shown).

Gene expression analysis revealed changes in the expression of genes involved in cholesterol export and import while the expression of genes involved in cholesterol synthesis remained unchanged (Supplementary Fig. 3). The expression of each HMG-CoA reductase (*Hmgcr*, involved in cholesterol synthesis) and *Srebp1* (encoding SREBP-1a and SREBP-1c transcription factors involved in the regulation of cholesterol and fatty acid synthesis) genes was unchanged (Sharpe and Brown, 2013). In contrast, the *Abca1* and *Npc2* genes, involved in extracellular export (Oram and Lawn, 2001) and lysosomal efflux of cholesterol (Cheruku *et al.*, 2006; Infante *et al.*, 2008), respectively, were significantly upregulated (4- and 2-fold, respectively) and *Ldlr* gene [which encodes the low-density lipoprotein (LDL) receptor involved in cholesterol cellular uptake; Posse De Chaves *et al.*, 2000] expression was decreased by 50%. *Apoe* gene (involved in cholesterol export out of the brain) expression was unchanged (Supplementary Fig. 3).

## Neuronal cholesterol accumulation increases the amyloid metabolism of APP and the phosphorylation of tau protein

Cholesterol enrichment in lipid rafts may facilitate the recruitment of APP and BACE1 to these microdomains and the production of β-CTF and amyloid-β peptides (von Arnim *et al.*, 2008; Cossec *et al.*, 2010; Marquer *et al.*, 2011). To determine if the inhibition of *Cyp46a1* gene expression affected the cholesterol and APP content of lipid rafts, we isolated hippocampal DRM microdomains on sucrose gradients: Fraction 2, enriched in flotillin, was biochemically identified as lipid rafts (Pike, 2004) (Fig. 2A). Inhibiting *Cyp46a1* gene expression was associated with a 1.3-fold increase in the cholesterol content and a 2.1-fold increased APP recruitment in the DRM (Fig. 2B) and affected the production of amyloid-β peptides. β-CTF and amyloid-$\beta_{42}$ in hippocampus had increased 3.4 ± 0.7 and 1.6 ± 0.14-fold, respectively, 3 weeks after AAV-shCYP46A1 vector injection; there was no change in the amyloid-$\beta_{40}$ level (Fig. 2C).

Amyloid-β is mostly produced in the trans-Golgi network and endosomes (Thinakaran and Koo, 2008) and enlarged endosomes are evident in the earliest stages of Alzheimer's disease before amyloid-β plaque deposition becomes obvious (Cataldo *et al.*, 2000). Increased neuronal cholesterol concentrations are associated *in vitro* with endosomal abnormalities (Cossec *et al.*, 2010). Endosomal trafficking was disturbed in CA3a pyramidal cells of mice injected with the AAV-shCYP46A1 vector, probably as a consequence of abnormal cholesterol metabolism: endosomes were 1.8 ± 0.27-fold more numerous and 6.3 ± 1.7-fold larger than in mice injected with the AAV-scramble vector (Fig. 2D).

We then studied the expression of phosphorylated glycogen synthase kinase 3-beta (GSK3β, ecoded by *Gsk3b*), the main tau kinase (Hoozemans *et al.*, 2009), and phosphorylated tau protein (encoded by *Mapt*). Three weeks after vector injection, 89 ± 5.8% of CA3a neurons of AAV-shCYP46A1-injected mice contained phosphorylated GSK3β (at Tyr216) and 95.8 ± 1.1% of CA3a neurons contained phosphorylated tau (p-tau at Thr231) (Fig. 2E). These phosphorylated forms were not detected after injection of the AAV-scramble vector (Fig. 2E). ELISA revealed a 6.75-fold increase in p-tau (at Thr181) in the hippocampus of AAV-shCYP46A1-injected mice (Fig. 2F). We found no evidence of tangles of paired helical filaments.

## Neuronal cholesterol accumulation induces endoplasmic reticulum stress in hippocampal neurons

*In vitro* studies in macrophages have reported that cholesterol accumulation induces endoplasmic reticulum stress (Feng *et al.*, 2003). We tested whether cholesterol accumulation in neurons due to downregulation of *Cyp46a1* gene expression caused stress in the endoplasmic reticulum. We analysed endoplasmic reticulum structure in CA3a neurons by electron microscopy 3 weeks after injection. Indeed, endoplasmic reticulum stress is revealed by changes its ultrastructure (Asselah *et al.*, 2010). The endoplasmic reticulum was swollen, dilated and disorganized with fine granular deposits observed in CA3a neurons in mice injected with the AAV-shCYP46A1 vector but not those in mice injected with the AAV-scramble vector (Fig. 3A, left panel). The CHOP protein (encoded by *Ddit3*) and the phosphorylated form of PERK (p-PERK, encoded by *Eif2ak3*) are markers of endoplasmic reticulum stress (Schroder and Kaufman, 2005). In the animals treated with the AAV-shCYP46A1 vector, 92.2 ± 1.4% of CA3a neurons contained p-PERK whereas p-PERK was evident only in 0.03 ± 0.02 % of neurons in mice injected with the AAV-scramble vector (Fig. 3A and B). The percentage of CA3a neurons containing CHOP protein was 75 ± 5.3% in AAV-shCYP46A1-injected mice and only 0.15 ± 0.1% in AAV-scramble-injected mice (Fig. 3A and B).

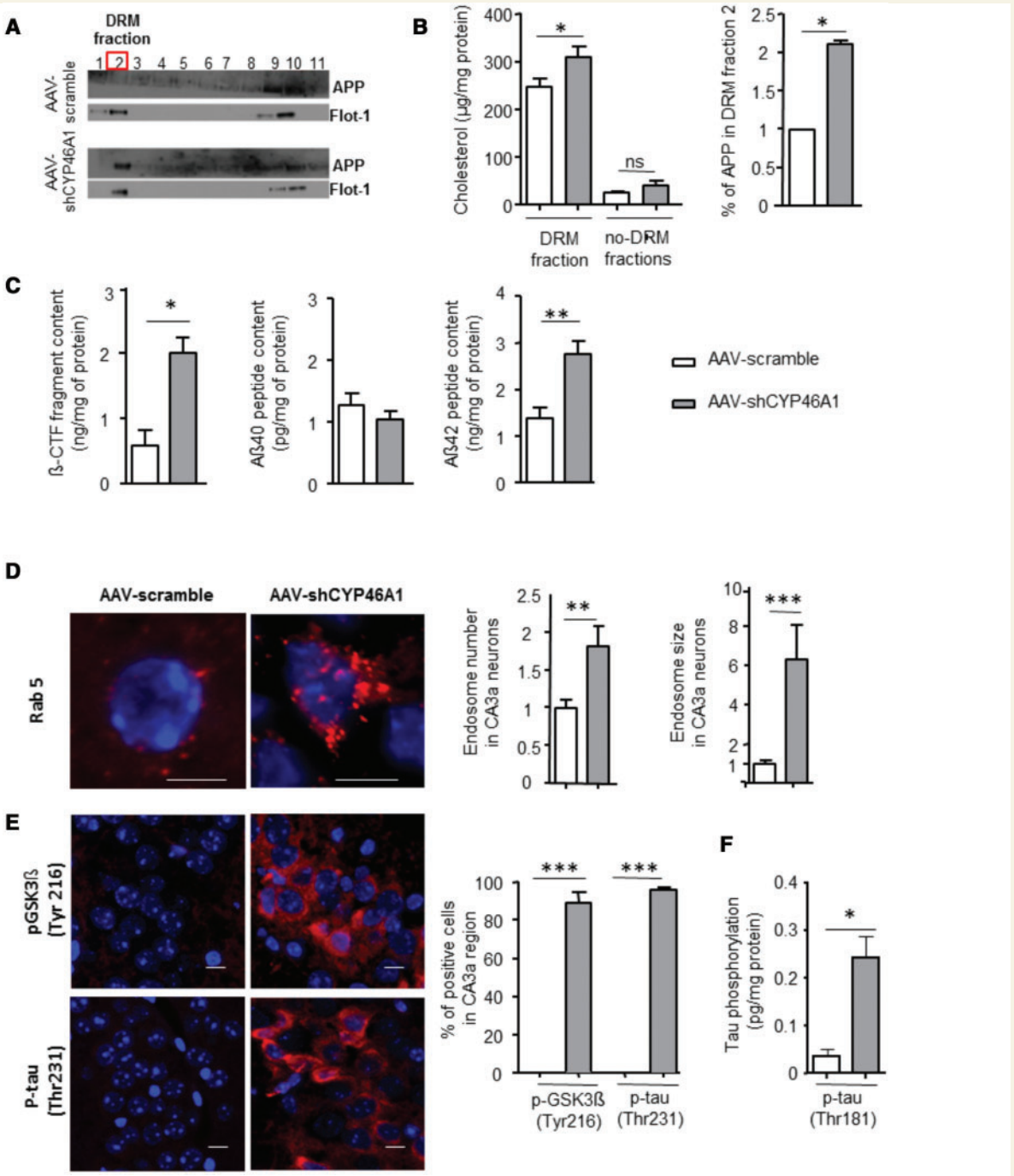


**Figure 2 Neuronal accumulation induced by the inhibition of *Cyp46a1* gene expression induces amyloid metabolism of APP, increased size and number of the endosomal compartment and tau phosphorylation.** (**A**) APP and flotillin 1 in hippocampi were analysed by western blotting with fractions collected from the top (Fraction 1) to the bottom of sucrose gradients. Fraction 2 enriched in flotillin 1 contains detergent-resistant membrane (DRM). (**B**) Cholesterol (*left*) and APP content (*right*) in DRM and non-DRM hippocampal fractions 3 weeks after injecting AAV-scramble or AAV-shCYP46A1 vectors. Reported APP levels in Fraction 2 (DRM) are normalized to those of APP in the same hippocampal fraction of AAV-scramble-injected mice. $^{*}P < 0.05$ by two-tailed unpaired *t*-test. ns = not significant. (**C**) ELISA quantification of hippocampal β-CTF and amyloid-$\beta_{40}$/amyloid-$\beta_{42}$ peptides 3 weeks after injecting AAV-scramble or AAV-shCYP46A1 vector ($n = 5$ mice per vector). $^{*}P < 0.05$ by two-tailed unpaired *t*-test. (**D**) *Left*: Rab5 immunostaining of CA3a neurons from AAV-scramble or AAV-shCYP46A1-injected mice (red, scale bar = 6 µm). *Right*: Numbers and sizes of endosomes from AAV-shCYP46A1-injected mice are normalized to values for AAV-scramble-injected mice (60 cells were counted in six sections per mouse, five mice per vector and per time point). $^{***}P < 0.0001$, two-tailed unpaired *t*-test). (**E**) *Left*: Percentage of CA3a pyramidal cells immunoreactive for phosphorylated GSK3β (p-GSK3β, at Tyr216) and phosphorylated tau (p-tau, at Thr231) in normal mice 3 weeks after injecting AAV-scramble or AAV-shCYP46A1 vector ($n = 5$ mice per vector and per time point, sections from three levels per mouse, two-tailed unpaired Student's *t*-test $^{***}P < 0.0001$). *Right*: Levels of phosphorylated tau at Thr181 in the hippocampus, 3 weeks after injecting AAV-scramble or AAV-shCYP46A1 vectors ($n = 4$–5 mice per group, two-tailed unpaired *t*-test $^{**}P < 0.01$). (**F**) ELISA quantification of hippocampal tau phosphorylated at Thr181, 3 weeks after injecting AAV-scramble or AAV-shCYP46A1 vector ($n = 5$ mice per vector, $^{*}P < 0.05$ by two-tailed unpaired *t*-test).

## Neuronal cholesterol accumulation induces apoptotic death of hippocampal neurons

Injection with the AAV-shCYP46A1 vector was followed by loss of CA3a pyramidal neurons. NeuN immunostaining revealed a 31 ± 3% reduction of CA3a neuronal density after 4 weeks and a 77 ± 4.5% reduction after 8 weeks; CA3a pyramidal cells were almost completely absent by 12 weeks (Fig. 4A and B). In the CA1 region where initial transgene expression was lower (Supplementary Fig. 2A), neuronal loss was slower (26.7 ± 10.7% at 8 weeks) and less extensive (62.3 ± 6.1% loss at 12 weeks) (Fig. 4A and B). Dying neurons showed apoptotic signs, notably shrinkage of the cell soma, presence of pyknotic nuclei (Fig. 4C, left panel) chromatin condensation, vacuoles and membrane blebs (Fig. 4C, right panel). Four weeks after injection of the AAV-shCYP46A1 vector, expression of caspase 12 protein had increased 3.8 ± 0.1-fold in CA3a hippocampal neurons (Fig. 4D and E). About 80% of CA3a neurons contained cleaved caspase 3 and cleaved caspase 9, both major actors of apoptosis (Fig. 4D and E). No apoptosis was detected in neurons of mice injected with the AAV-scramble vector (Fig. 4C–E). Thus, *Cyp46a1* inhibition and consequent neuronal cholesterol accumulation in hippocampus led to rapid and progressive apoptotic neuronal loss in C57Bl/6 mice.

## Neuronal cholesterol overload induces cognitive impairment and hippocampal atrophy

We then evaluated the consequences of the neuronal toxicity associated with cholesterol accumulation on mouse behaviour 8 weeks after injection of the vectors.

The exploratory activity of mice injected with the AAV-shCYP46A1 vector was greater than that of control AAV-scramble mice (Fig. 5A, left); with a longer daily distance travelled (Fig. 5A, right) largely due to increased nocturnal exploration; this is consistent with previous observations of transgenic mouse models of Alzheimer's disease (Faure *et al.*, 2011). In the open-field task, there was a trend for AAV-shCYP46A1 mice to spend more time than control mice at the periphery (data not shown) resulting in a higher periphery/centre ratio (Fig 5B, left). Distance travelled in the open-field task was not different between the groups of mice (data not shown), the correlation between actimeter and open-field assay results (Fig 5B, right) strongly suggests that injection with AAV-shCYP46A1 altered emotional behaviour rather than caused motor impairment.

In the Morris water maze test, the distance travelled to find the platform was shorter for AAV-scramble than AAV-shCYP46A1-injected animals (Fig. 5C, left). In the probe test, where the platform was removed, AAV-scramble-injected animals displayed a strong preference for the targeted quadrant, whereas AAV-shCYP46A1-injected mice did not, indicative of memory impairment ($n$ = 9/10 per group, Fig. 5C, right).

MRI 12 weeks after vector injection revealed that the total hippocampal volume was 13.7 ± 2.6% smaller in AAV-shCYP46A1-injected than AAV-scramble-injected animals (Fig 5D).

Thus, the decrease of cholesterol-24-hydroxylase activity, the consequent cholesterol accumulation and neuronal death were associated with impaired cognitive abilities and hippocampal atrophy in C57Bl/6 mice.

## Cholesterol accumulation in the hippocampus exacerbates the phenotype of APP23 mice

We tested whether the inhibition of *Cyp46a1* gene expression in hippocampal neurons of a mouse model of Alzheimer's disease aggravated the phenotype. The transgenic mouse line APP23 (Thy1-hAPPswe) overexpresses the human $APP_{751}$ gene, which carries the Swedish double mutation (K670N-M671L) associated with familial forms of Alzheimer's disease (Sturchler-Pierrat and Staufenbiel, 2000). APP23 mice produce progressive, increasing amounts of amyloid-β peptides from birth, and both memory deficits and amyloid plaques develop during ageing (Sturchler-Pierrat and Staufenbiel, 2000). We first compared the effects of *Cyp46a1* gene inhibition on brain cholesterol in APP23 and normal mice. APP23 mice were injected with AAV-scramble and AAV-ShCYP46A1 at 5 months of age. The distribution and intensity of enhanced GFP expression (data not shown), the reduction in *Cyp46a1* gene expression (Fig. 6A) and the increase in cholesterol content within the brain (Fig. 6B) were comparable in the two mouse lines.

Amyloid-$\beta_{40}$ and amyloid-$\beta_{42}$ contents were 3.8- and 2.9-fold higher, respectively, 4 weeks after the injection in AAV-shCYP46A1 than AAV-scramble mice (Fig. 6C). No difference in amyloid plaques was observed ($n$ = 10 mice). CA3a neurons (88 ± 2.8%) of AAV-shCYP46A1-injected mice expressed phosphorylated tau (at Thr231) (Fig. 6D). Tau phosphorylation (at Thr181) in the hippocampus was 350% higher in AAV-shCYP46A1-injected than AAV-scramble-injected APP23 mice (Fig. 6E).

Neuronal death in APP23 mice has been reported to be minimal, even at 18 months (Bondolfi *et al.*, 2002). However, AAV-shCYP46A1 injection promoted a rapid and marked hippocampal neuronal loss in CA3a and CA1 regions (Fig. 6F) whereas AAV-scramble injection did not affect neuronal survival (data not shown). Neuronal loss after *Cyp46a1* gene downregulation was more marked in APP23 mice than in normal animals (Fig. 6F): 4 weeks after AAV-shCYP46A1 injection neuronal death was 2.2-fold more prevalent in CA3a and 10.6-fold more prevalent in the CA1 region of APP23 mice (Fig. 6G). These observations are consistent with the

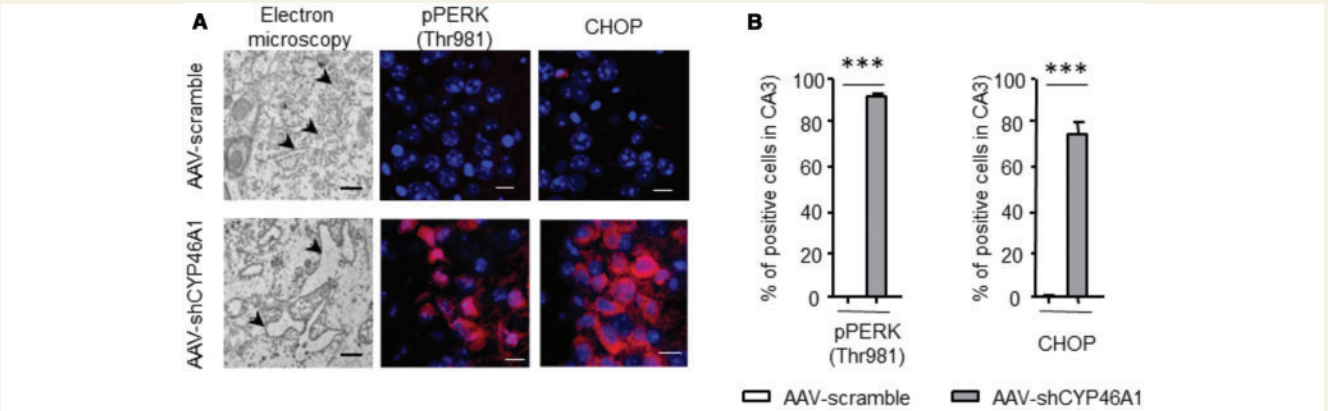


**Figure 3 Neuronal cholesterol accumulation induced by inhibition of *Cyp46a1* gene expression triggers endoplasmic reticulum stress.** (**A**) Electron micrographs of endoplasmic reticulum in CA3a neurons from normal mice 4 weeks after injecting AAV-scramble or AAV-shCYP46A1 vector. Endoplasmic reticulum from AAV-scramble-injected mice has normal morphology with cisternae organized in thin stacks (*left*; black arrows). Endoplasmic reticulum stacks in AAV-shCYP46A1-injected animals are swollen and dilated (*right*; scale bar = 1 μm). (**B**) *Left*: CA3a pyramidal neuron immunostaining of phosphorylated PERK (p-PERK) and CHOP 3 weeks after injecting AAV-scramble or AAV-shCYP46A1 vectors. Scale bar = 50 μm. *Right*: Percentage of CA3a neurons that are p-PERK and CHOP immuno-positive 3 weeks after injecting AAV-scramble or AAV-shCYP46A1 vectors into normal mice (normalized to values for CA3 cells from AAV-scramble-injected mice, $n = 5$ mice per vector per time point; three sections per mouse). ***$P < 0.0001$; two-tailed unpaired *t*-test.

toxic consequences of cholesterol-24-hydroxylase inhibition being exacerbated in the context of amyloid accumulation.

# Discussion

Impairment of cerebral cholesterol homeostasis has been described in several neurodegenerative disorders, including Alzheimer's disease, Parkinson's disease and Huntington's disease (Vance, 2012). However, the role of *in vivo* cholesterol abnormalities in the neurodegeneration process is not clear. In the adult brain, cholesterol is synthesized essentially by astrocytes and shuttles to neurons where its abundance is tightly regulated (Dietschy and Turley, 2004). Cholesterol in excess cannot freely cross the blood–brain barrier and its extrusion from the brain therefore involves its hydroxylation by cholesterol-24-hydroxylase, an enzyme encoded by the *Cyp46a1* gene. The resulting 24S-hydroxycholesterol crosses the blood–brain barrier and is metabolized in the liver (Dietschy and Turley, 2004; Russell *et al.*, 2009). The expression of cholesterol 24-hydroxylase has been reported to be abnormal in the brain of patients with Alzheimer's disease (Bogdanovic *et al.*, 2001).

In transgenic mice in which the *Cyp46a1* gene is knocked down, the cholesterol content remains normal: the absence of *Cyp46a1* gene expression from an early developmental stage is compensated by a homeostatic adaptation of cholesterol metabolism by modulation of cholesterol synthesis (Lund *et al.*, 2003; Xie *et al.*, 2003; Shafaati *et al.*, 2011). We therefore used an alternative approach based on the injection of an AAV vector carrying a *Cyp46a1*-specific shRNA into the hippocampus of adult mice to inhibit *Cyp46a1* gene expression. The hippocampus is a vulnerable cerebral region, affected early in patients with Alzheimer's disease (Leal and Yassa, 2013). The sequence used (sh271) was selected from 11 sequences by *in vitro* and *in vivo* screening for efficient inhibition of cholesterol 24-hydroxylase expression and activity, without off-target consequences of RNA interference.

The injection of AAV-shCYP46A1 into the mouse hippocampus resulted in stable transgene expression in pyramidal neurons causing decreased expression of *Cyp46a1* and cholesterol 24-hydroxylase. As a consequence, there was a significant decrease of 24S-hydroxycholesterol and a significant increase of cholesterol at biochemical and cellular levels in the hippocampus.

Expression of the *Hmgcr* and *Srebp* genes was unchanged, suggesting that cholesterol synthesis was not modified. However, the expression of *Abca1* involved in cholesterol export was increased and expression of *Ldlr* involved in cholesterol import was decreased, as observed in cholesterol-overloaded macrophages, presumably to reduce cholesterol intake and enhance its cellular efflux (Tabas, 2002). Thus, the accumulation of cholesterol in AAV-shCYP46A1-injected mice was not due to an increase of its synthesis but solely from the reduced efflux.

*In vitro*, amyloidogenic processing of APP was found to be linked to cholesterol distribution in lipid rafts (Cossec *et al.*, 2010). APP is preferentially processed within cholesterol and sphingolipid-enriched lipid rafts, membrane microdomains where APP encounters β- and γ-secretases (Vetrivel and Thinakaran, 2006). APP cleavage by BACE1 and γ-secretase produces β-CTF and amyloid-β peptides (amyloid-$\beta_{40}$ and amyloid-$\beta_{42}$) (von Arnim *et al.*, 2008; Cossec *et al.*, 2010; Marquer *et al.*, 2011).

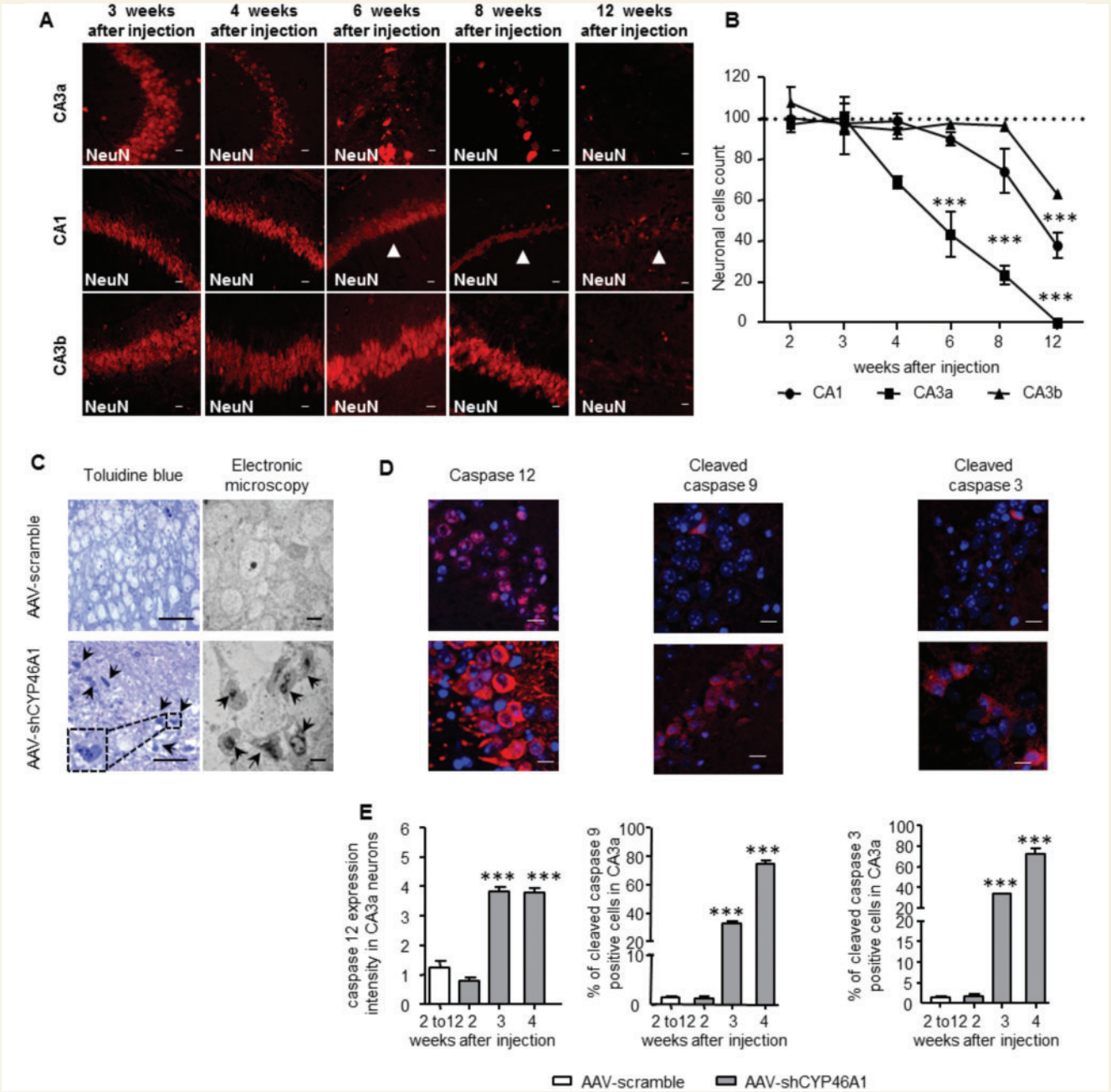


**Figure 4 Neuronal cholesterol accumulation induced by downregulation of *Cyp46a1* gene expression causes apoptotic neuronal death**. (**A**) Neuronal loss (NeuN immunostaining in red) in the CA1 (arrowheads), CA3a and b regions of AAV-shCYP46A1-injected mice 3 to 12 weeks after injection. Scale bar = 50 μm. (**B**) Numbers of NeuN-positive cells were counted from 2 to 12 weeks in AAV-shCYP46A1-injected mice (from three sections in five mice per vector and time point). The values reported are normalized to NeuN-positive cell counts in mice injected with the AAV-scramble vector (two-way ANOVA: effect of vector time and interaction between time and vector ***$P < 0.0001$). (**C**) *Left*: Photomicrographs of Toluidine blue-stained semi-thin slices of the CA3a region from normal mice 4 weeks after injecting AAV-scramble or AAV-shCYP46A1 vector. Black arrows show degenerating neurons with pyknotic nuclei (high magnification inset, scale bar = 50 μm). *Right*: Electron micrographs of the CA3a region in normal mice after injecting the same vectors. Black arrows show neurons in the terminal stages of apoptosis, with substantial morphological irregularities, nuclear chromatin condensation and membrane blebbing (lower right inset, scale bar = 10 μm). (**D**) CA3a region immunostained (red) with caspase 12, cleaved caspase 9 or cleaved caspase 3 antibodies 4 weeks after injecting AAV-scramble or AAV-shCYP46A1 vectors. Scale bar = 20 μm. (**E**) Intensity of caspase 12 immunoreactivity and percentage of cleaved caspase 9 or cleaved caspase 3 immuno-positive CA3 pyramidal cells in normal mice injected with the AAV-scramble (2 to 12 weeks after injection) or AAV-shCYP46A1 (2 to 4 weeks after injection) vector ($n = 5$ mice per vector per time point, three sections per mouse). ***$P < 0.0001$ by one-way ANOVA with Newman-Keuls *post hoc* test.

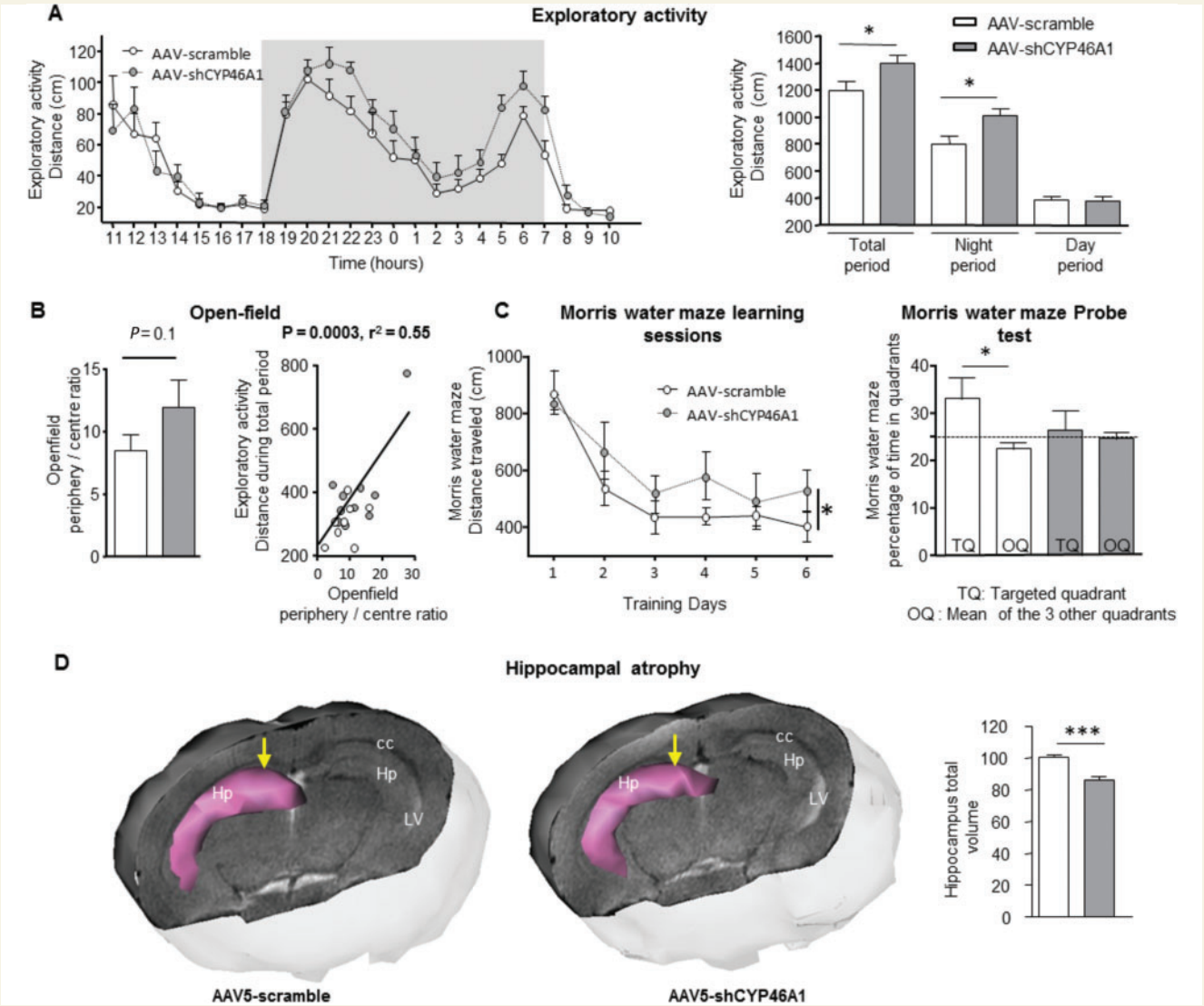


**Figure 5 Cyp46a1 downregulation triggers memory deficits and hippocampal atrophy.** (**A**) Exploratory activity assessed by 24 h actimetry, 8 weeks after injecting AAV-scramble or AAV-shCYP46A1 vectors ($n$ = 10 mice per group). Mean distance travelled every hour (*left*: vector effect $^{**}P < 0.005$, time effect $^{***}P < 0.0001$ by two-way ANOVA with repeated measures) and mean distance travelled during day or night periods (right, $^{*}P < 0.05$, two-tailed unpaired $t$-test). (**B**) *Left*: Periphery:centre ratio in open-field for AAV-scramble and AAV-shCYP46A1 mice, 8 weeks after injection ($n$ = 8 mice per vector). *Right*: Correlation between the periphery:centre ratio in open-field and the total distance in 24 h actimetry (Pearson correlation test: $r^2 = 0.55$, $P = 0.0003$). (**C**) *Left*: Path length (mean ± SEM) during the learning session to reach the hidden platform. $^{*}P < 0.05$, two-way ANOVA with repeated measures. *Right*: Percentage of time spent in targeted quadrant (TQ) and in other quadrants (OQ) during the probe test (two-tailed unpaired $t$-test, $^{*}P < 0.05$). (**D**) *In vivo* MRI scans of AAV-scramble- and AAV-shCYP46A1-injected animals, 12 weeks after injection of the vectors. Three dimensional views of the regions used to quantify hippocampal volumes are outlined in purple. The total hippocampal volumes are lower in AAV-shCYP46A1-injected mice than AAV-scramble-injected mice (volumes normalized to that of AAV-scramble injected mice, $n$ = 7 mice per group, $^{***}P < 0.0001$, two-tailed unpaired $t$-test). cc = corpus callosum; Hp = hippocampus; LV = lateral ventricle.

Our results confirm that an increased neuronal cholesterol load *in vivo*, especially in lipid rafts, stimulates the APP amyloidogenic pathway with overproduction of amyloid-β peptides.

Cholesterol accumulation associated with AAV-shCYP46A1 injection was accompanied by modifications of the endosomal compartment in affected neurons. This confirms *in vitro* observations that increased neuronal cholesterol abundance is associated with endosomal abnormalities (Cossec *et al.*, 2010). Interestingly, enlarged endosomes are evident during the earliest stages of Alzheimer's disease, before amyloid plaque deposition is obvious (Cataldo *et al.*, 2000). These observations suggest that cholesterol accumulation *in vivo* following downregulation of *Cyp46a1* may promote the generation of amyloid-β peptides through both the recruitment of APP in lipid

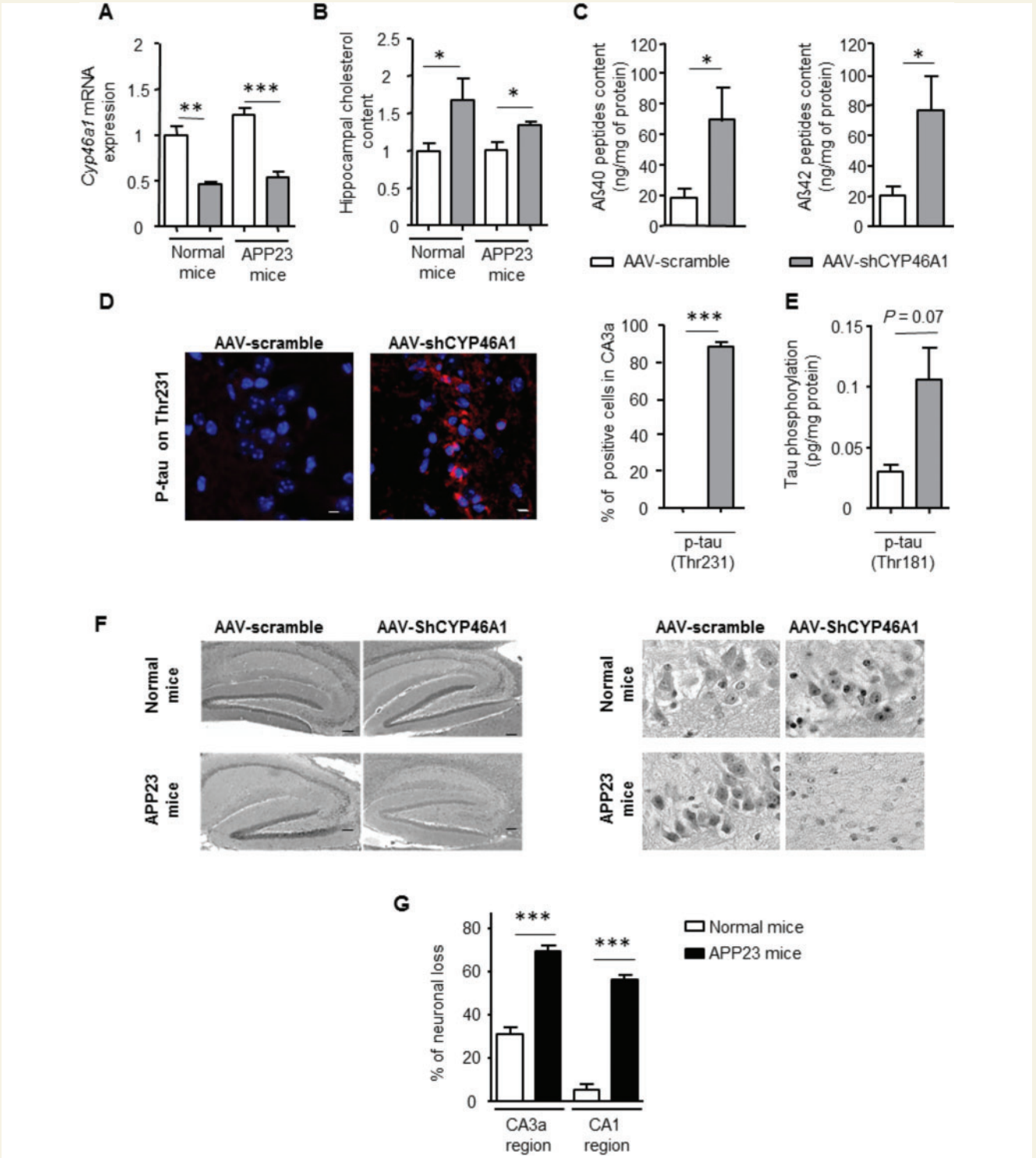


**Figure 6 Cholesterol accumulation following *Cyp46a1* downregulation leads to phenotypic aggravation in APP23 mice: increased amyloid-β peptide accumulation, tau phosphorylation and severe neuronal death.** (**A**) Measurements of the expression of the *Cyp46a1* gene in normal and APP23 mouse hippocampus 4 weeks after injecting the AAV-shCYP46A1 vector [values normalized to those in AAV-scramble-injected normal (C57BL/6) mice, $n = 5$ mice per vector, $^{**}P < 0.005$ and $^{***}P < 0.0001$ by one-way ANOVA with Newman-Keuls *post hoc* test]. (**B**) Cholesterol content in APP23 and normal (C57Bl/6) mouse hippocampus 4 weeks after injecting the AAV-shCYP46A1 vector [values normalized to those in AAV-scramble-injected normal (C57BL/6 mice, $n = 5$ mice per vector, $^{*}P < 0.05$ by one-way ANOVA with Newman-Keuls *post hoc* test]. (**C**) Amyloid-$\beta_{40}$ and amyloid-$\beta_{42}$ contents in APP23 mouse hippocampus 4 weeks after injecting AAV-scramble or AAV-CYP46A1 vector ($n = 5$ mice per vector). $^{***}P < 0.0001$ by two-tailed unpaired *t*-test. (**D**) *Left*: Immunostaining of phosphorylated tau (red, Thr231) in hippocampus of APP23 mice 4 weeks after injecting AAV-scramble or AAV-shCYP46A1 vector. Scale bar = 50 μm. *Right*: Percentages of p-tau (Thr 231)-positive CA3a pyramidal cells in APP23 mice 4 weeks after injecting AAV-scramble or AAV-shCYP46A1 vectors ($n = 5$ mice per

(continued)

rafts and the increased endosomal compartment that favours the recycling of APP from the cell surface.

There is still debate about the consequences of cholesterol accumulation on tau levels and on its metabolism (especially its phosphorylation). Here, we show that accumulation of cholesterol *in vivo* is associated with increased tau phosphorylation. We did not find evidence for the presence of tangles but it remains unclear whether murine phosphorylated tau can aggregate in the same way as human tau (Ando *et al.*, 2011).

Downregulation of *Cyp46a1* expression and consequent cholesterol accumulation led to neuronal death; the neurons presented shrinkage of the cell soma, presence of pyknotic nuclei and caspase activation, all known to be signs of apoptosis (Elmore, 2007). Interestingly, cholesterol accumulation, increased production of amyloid-$\beta_{42}$ peptides and phosphorylated tau were observed before neuronal death in mice injected with the AAV-shCYP46A1 vector. Amyloid peptides and tau phosphorylation could indeed contribute to mechanisms of neuronal death (Mattson *et al.*, 1998; Nakagawa *et al.*, 2000; Canevari *et al.*, 2004; Mondragon-Rodriguez *et al.*, 2013). Endoplasmic reticulum stress has recently been identified as a deleterious process contributing to neurodegeneration (Hetz and Mollereau, 2014). Consistent with findings for macrophages *in vitro* (Feng *et al.*, 2003), our data show that an accumulation of cholesterol in the brain may trigger endoplasmic reticulum stress that may in turn contribute to neurodegeneration or aggravate the neuronal death induced by neurodegenerative processes. Others mechanisms than endoplasmic reticulum stress contributing to induce neuronal death cannot however be excluded. This neuronal death was accompanied by a reduction of the hippocampal volume and by behavioural/cognitive changes. A similar structure-functional relationship between hippocampal damage and memory loss has been described in patients with Alzheimer's disease (Fox *et al.*, 1999; Mueller *et al.*, 2010).

Our observations of normal mice suggested that high intraneuronal cholesterol concentrations may aggravate pathological changes in amyloid models of Alzheimer's disease. We therefore investigated the consequences of *Cyp46a1* downregulation in APP23 mice. This animal model exhibits amyloid pathology and memory deficits but no neuronal death (Bondolfi *et al.*, 2002) or phosphorylation of tau (Sturchler-Pierrat and Staufenbiel, 2000). In APP23 mice injected with AAV-shCYP46A1, the cholesterol abundance in hippocampal neurons and amyloid-β production were both high and coupled to tau phosphorylation. The prevalence of neuronal death was substantially higher in these APP23 mice than in normal mice with the same increase in neuronal cholesterol content. However, we did not find evidence that intraneuronal accumulation of cholesterol increased, at least in the short term, the formation of amyloid plaques in APP23 mice. These mice exhibited 60% mortality rate 3 months after the injection of AAV-shCYP46A1 vector, likely due to the severe neuronal loss. This precluded to determine whether, in the long term, the accumulation of cholesterol in neurons favoured not only the production of amyloid-β peptides but also of amyloid plaques and paired helical filaments. As always, results obtained in mouse models must be discussed with caution. The increase in neuronal cholesterol that was obtained in normal and APP23 mice following the injection of AAV-shCYP46A1 vector was very marked and occurred rapidly, a situation that occurs unlikely in patients with Alzheimer's disease. In addition, it is probable that neuronal cell death resulted more from the major and generalized cellular dysfunction induced by cholesterol increase than from the accumulation of amyloid-β peptides *per se*.

Despite the limitations of our mouse models, this work reveals a pivotal role for cholesterol accumulation in the amyloid-β peptide accumulation and the abnormal phosphorylation of tau, two events that characterize early stage of Alzheimer's disease.

These results also suggest that cholesterol accumulation could sensitize neurons to death induced by amyloid pathology. Amyloid pathology is known to occur at least 20 years before the onset of clinical symptoms of Alzheimer's disease (Sperling *et al.*, 2011; Jack *et al.*, 2013). In the context of high amyloid load, the occurrence of neuronal cholesterol accumulation could contribute to initiate or aggravate the neurodegenerative process. Cholesterol levels decline by 40% in the healthy ageing brain (Thelen *et al.*, 2006). However, increased cholesterol levels have been observed in vulnerable brain regions of patients with Alzheimer's disease (Cutler *et al.*, 2004; Lazar *et al.*, 2013). Moreover, when the integrity of the blood–brain barrier is compromised by vascular injury, e.g. in atherosclerosis, the regulated entry of cholesterol-carrying lipoproteins into the brain may be impaired and result in accumulation of membrane cholesterol. By favouring the amyloid processing of APP and the abnormal phosphorylation of tau, the accumulation of cholesterol both in neurons and endothelial cells could act in synergy with other mechanisms that induce amyloid deposits and the

**Figure 6** Continued

vector, three sections per mouse, two-tailed unpaired *t*-test ***$P < 0.0001$). (**E**) ELISA quantification of hippocampal tau phosphorylated at Thr181 in APP23 mouse hippocampus 4 weeks after injecting AAV-scramble or AAV-shCYP46A1 vectors ($n = 5$ mice per group, two-tailed unpaired *t*-test). (**F**) Haematein eosin-stained sections of CA3a region from normal (C57BL/6) and APP23 mice 4 weeks after the injection of AAV-shCYP46A1 or AAV-scramble vectors. Scale bar = 50 μm. (**G**) Neuronal loss in the CA3a and CA1 regions of normal (C57Bl/6) and APP23 mice 4 weeks after injecting the AAV-shCYP46A1 vector (three sections from each of five mice per group, ***$P < 0.0001$ by unpaired two-tailed *t*-test).

formation of neurofibrillary tangles and then aggravate the neurodegenerative process of Alzheimer's disease (Casserly and Topol, 2004; Silvestrini *et al.*, 2011; Wendell *et al.*, 2012; Sadleir *et al.*, 2013). Thus, interventions to decrease brain cholesterol may provide a therapeutic brake to slow-down the overall neurodegenerative process of Alzheimer's disease. In line with this hypothesis we recently showed that increasing *Cyp46a1* gene expression in the brain of Alzheimer's disease mouse models significantly reduces the severity of their amyloid pathology and memory deficits (Hudry *et al.*, 2010).

## Acknowledgements

We thank Peter P. De Deyn and Debby Van Dam for their contributions to mouse evaluation, Abdellatif Benraiss for his help in designing the sh-RNA strategy, R.D. Palmiter for providing the Znt3 antibody the Cell Imaging Platform of the Institut du Cerveau et de la Moelle (ICM, Paris), Mathias Staufenbiel for providing the APP23 mouse line, Françoise Fouquet, Sylvie Guidoux, and Laetitia Breton for their excellent technical assistance. We thank Pierre Bougnères for help in editing this manuscript.

## Funding

This work was supported by the Fondation France Alzheimer, the Fondation pour la Recherche Médicale, the Fondation Del Ducca, the Fondation de l'Avenir, the Fondation pour la Recherche sur le Cerveau, the Investissements d'avenir ANR-10-IAIHU-06 and the ANR-10-MALZ-013 CholAD.

## Supplementary material

Supplementary material is available at *Brain* online.

## References

Ando K, Leroy K, Heraud C, Yilmaz Z, Authelet M, Suain V, et al. Accelerated human mutant tau aggregation by knocking out murine tau in a transgenic mouse model. Am J Pathol 2011; 178: 803–16.

Asselah T, Bieche I, Mansouri A, Laurendeau I, Cazals-Hatem D, Feldmann G, et al. *In vivo* hepatic endoplasmic reticulum stress in patients with chronic hepatitis C. J Pathol 2010; 221: 264–74.

Ayciriex S, Regazzetti A, Gaudin M, Prost E, Dargere D, Massicot F, et al. Development of a novel method for quantification of sterols and oxysterols by UPLC-ESI-HRMS: application to a neuroinflammation rat model. Anal Bioanal Chem 2012; 404: 3049–59.

Bauer M, Kinkl N, Meixner A, Kremmer E, Riemenschneider M, Forstl H, et al. Prevention of interferon-stimulated gene expression using microRNA-designed hairpins. Gene Ther 2009; 16: 142–7.

Bieche I, Lerebours F, Tozlu S, Espie M, Marty M, Lidereau R. Molecular profiling of inflammatory breast cancer: identification of a poor-prognosis gene expression signature. Clin Cancer Res 2004; 10: 6789–95.

Bjorkhem I. Crossing the barrier: oxysterols as cholesterol transporters and metabolic modulators in the brain. J Intern Med 2006; 260: 493–508.

Bjorkhem I, Lutjohann D, Diczfalusy U, Stahle L, Ahlborg G, Wahren J. Cholesterol homeostasis in human brain: turnover of 24S-hydroxycholesterol and evidence for a cerebral origin of most of this oxysterol in the circulation. J Lipid Res 1998; 39: 1594–600.

Bogdanovic N, Bretillon L, Lund EG, Diczfalusy U, Lannfelt L, Winblad B, et al. On the turnover of brain cholesterol in patients with Alzheimer's disease. Abnormal induction of the cholesterol-catabolic enzyme CYP46 in glial cells. Neurosci Lett 2001; 314: 45–8.

Bondolfi L, Calhoun M, Ermini F, Kuhn HG, Wiederhold KH, Walker L, et al. Amyloid-associated neuron loss and gliogenesis in the neocortex of amyloid precursor protein transgenic mice. J Neurosci 2002; 22: 515–22.

Canevari L, Abramov AY, Duchen MR. Toxicity of amyloid beta peptide: tales of calcium, mitochondria, and oxidative stress. Neurochem Res 2004; 29: 637–50.

Casserly I, Topol E. Convergence of atherosclerosis and Alzheimer's disease: inflammation, cholesterol, and misfolded proteins. Lancet 2004; 363: 1139–46.

Cataldo AM, Peterhoff CM, Troncoso JC, Gomez-Isla T, Hyman BT, Nixon RA. Endocytic pathway abnormalities precede amyloid beta deposition in sporadic Alzheimer's disease and Down syndrome: differential effects of APOE genotype and presenilin mutations. Am J Pathol 2000; 157: 277–86.

Cheruku SR, Xu Z, Dutia R, Lobel P, Storch J. Mechanism of cholesterol transfer from the Niemann-Pick type C2 protein to model membranes supports a role in lysosomal cholesterol transport. J Biol Chem 2006; 281: 31594–604.

Cooper NG, McLaughlin BJ. The distribution of filipin-sterol complexes in photoreceptor synaptic membranes. J Comp Neurol 1984; 230: 437–43.

Cossec JC, Simon A, Marquer C, Moldrich RX, Leterrier C, Rossier J, et al. Clathrin-dependent APP endocytosis and Abeta secretion are highly sensitive to the level of plasma membrane cholesterol. Biochim Biophys Acta 2010; 1801: 846–52.

Cutler RG, Kelly J, Storie K, Pedersen WA, Tammara A, Hatanpaa K, et al. Involvement of oxidative stress-induced abnormalities in ceramide and cholesterol metabolism in brain aging and Alzheimer's disease. Proc Natl Acad Sci USA 2004; 101: 2070–5.

Dietschy JM, Turley SD. Cholesterol metabolism in the brain. Curr Opin Lipidol 2001; 12: 105–12.

Dietschy JM, Turley SD. Thematic review series: brain Lipids. Cholesterol metabolism in the central nervous system during early development and in the mature animal. J Lipid Res 2004; 45: 1375–97.

Elmore S. Apoptosis: a review of programmed cell death. Toxicol Pathol 2007; 35: 495–16.

Faure A, Verret L, Bozon B, El Tannir El Tayara N, Ly M, et al. Impaired neurogenesis, neuronal loss, and brain functional deficits in the APPxPS1-Ki mouse model of Alzheimer's disease. Neurobiol Aging 2011; 32: 407–18.

Feng B, Yao PM, Li Y, Devlin CM, Zhang D, Harding HP, et al The endoplasmic reticulum is the site of cholesterol-induced cytotoxicity in macrophages. Nat Cell Biol 2003; 5: 781–92.

Fox NC, Scahill RI, Crum WR, Rossor MN. Correlation between rates of brain atrophy and cognitive decline in AD. Neurology 1999; 52: 1687–9.

Grimm D, Streetz KL, Jopling CL, Storm TA, Pandey K, Davis CR, et al. Fatality in mice due to oversaturation of cellular microRNA/short hairpin RNA pathways. Nature 2006; 441: 537–41.

Hetz C, Mollereau B. Disturbance of endoplasmic reticulum proteostasis in neurodegenerative diseases. Nat Rev Neurosci 2014; 15: 233–49.

Hoozemans JJ, van Haastert ES, Nijholt DA, Rozemuller AJ, Eikelenboom P, Scheper W. The unfolded protein response is activated in pretangle neurons in Alzheimer's disease hippocampus. Am J Pathol 2009; 174: 1241–51.

Hudry E, Van Dam D, Kulik W, De Deyn PP, Stet FS, Ahouansou O, et al. Adeno-associated virus gene therapy with cholesterol 24-hydroxylase reduces the amyloid pathology before or after the onset of amyloid plaques in mouse models of Alzheimer's disease. Mol Ther 2010; 18: 44–53.

Infante RE, Wang ML, Radhakrishnan A, Kwon HJ, Brown MS, Goldstein JL. NPC2 facilitates bidirectional transfer of cholesterol between NPC1 and lipid bilayers, a step in cholesterol egress from lysosomes. Proc Natl Acad Sci USA 2008; 105: 15287–92.

Ishizuka N, Cowan WM, Amaral DG. A quantitative analysis of the dendritic organization of pyramidal cells in the rat hippocampus. J Comp Neurol 1995; 362: 17–45.

Jack CR Jr, Knopman DS, Jagust WJ, Petersen RC, Weiner MW, Aisen PS, et al. Tracking pathophysiological processes in Alzheimer's disease: an updated hypothetical model of dynamic biomarkers. Lancet Neurol 2013; 12: 207–16.

Lazar AN, Bich C, Panchal M, Desbenoit N, Petit VW, Touboul D, et al. Time-of-flight secondary ion mass spectrometry (TOF-SIMS) imaging reveals cholesterol overload in the cerebral cortex of Alzheimer disease patients. Acta Neuropathol 2013; 125: 133–44.

Leal SL, Yassa MA. Perturbations of neural circuitry in aging, mild cognitive impairment, and Alzheimer's disease. Ageing Res Rev 2013; 12: 823–31.

Lund EG, Guileyardo JM, Russell DW. cDNA cloning of cholesterol 24-hydroxylase, a mediator of cholesterol homeostasis in the brain. Proc Natl Acad Sci USA 1999; 96: 7238–43.

Lund EG, Xie C, Kotti T, Turley SD, Dietschy JM, Russell DW. Knockout of the cholesterol 24-hydroxylase gene in mice reveals a brain-specific mechanism of cholesterol turnover. J Biol Chem 2003; 278: 22980–8.

Lutjohann D, Bjorkhem I, Locatelli S, Dame C, Schmolling J, von Bergmann K, et al. Cholesterol dynamics in the foetal and neonatal brain as reflected by circulatory levels of 24S-hydroxycholesterol. Acta Paediatr 2001; 90: 652–7.

Lutjohann D, Breuer O, Ahlborg G, Nennesmo I, Siden A, Diczfalusy U, et al. Cholesterol homeostasis in human brain: evidence for an age-dependent flux of 24S-hydroxycholesterol from the brain into the circulation. Proc Natl Acad Sci USA 1996; 93: 9799–804.

Marquer C, Devauges V, Cossec JC, Liot G, Lecart S, Saudou F, et al. Local cholesterol increase triggers amyloid precursor protein-Bace1 clustering in lipid rafts and rapid endocytosis. FASEB J 2011; 25: 1295–305.

Mattson MP, Partin J, Begley JG. Amyloid beta-peptide induces apoptosis-related events in synapses and dendrites. Brain Res 1998; 807: 167–76.

Mondragon-Rodriguez S, Perry G, Zhu X, Moreira PI, Acevedo-Aquino MC, Williams S. Phosphorylation of tau protein as the link between oxidative stress, mitochondrial dysfunction, and connectivity failure: implications for Alzheimer's disease. Oxid Med Cell Longev 2013; 2013: 940603.

Mueller SG, Schuff N, Yaffe K, Madison C, Miller B, Weiner MW. Hippocampal atrophy patterns in mild cognitive impairment and Alzheimer's disease. Hum Brain Mapp 2010; 31: 1339–47.

Nakagawa T, Zhu H, Morishima N, Li E, Xu J, Yankner BA, Yuan J. Caspase-12 mediates endoplasmic-reticulum-specific apoptosis and cytotoxicity by amyloid-beta. Nature 2000; 403: 98–103.

Oram JF, Lawn RM. ABCA1. The gatekeeper for eliminating excess tissue cholesterol. J Lipid Res 2001; 42: 1173–9.

Palmiter RD, Cole TB, Quaife CJ, Findley SD. ZnT-3, a putative transporter of zinc into synaptic vesicles. Proc Natl Acad Sci USA 1996; 93: 14934–9.

Pike LJ. Lipid rafts: heterogeneity on the high seas. Biochem J 2004; 378: 281–92.

Posse De Chaves EI, Vance DE, Campenot RB, Kiss RS, Vance JE. Uptake of lipoproteins for axonal growth of sympathetic neurons. J Biol Chem 2000; 275: 19883–90.

Russell DW, Halford RW, Ramirez DM, Shah R, Kotti T. Cholesterol 24-hydroxylase: an enzyme of cholesterol turnover in the brain. Annu Rev Biochem 2009; 78: 1017–40.

Sadleir KR, Bennett DA, Schneider JA, Vassar R. Elevated Abeta42 in aged, non-demented individuals with cerebral atherosclerosis. Curr Alzheimer Res 2013; 10: 785–9.

Schroder M, Kaufman RJ. The mammalian unfolded protein response. Annu Rev Biochem 2005; 74: 739–9.

Sevin C, Benraiss A, Van Dam D, Bonnin D, Nagels G, Verot L, et al. Intracerebral adeno-associated virus-mediated gene transfer in rapidly progressive forms of metachromatic leukodystrophy. Hum Mol Genet 2006; 15: 53–64.

Shafaati M, Olin M, Bavner A, Pettersson H, Rozell B, Meaney S, et al. Enhanced production of 24S-hydroxycholesterol is not sufficient to drive liver X receptor target genes *in vivo*. J Intern Med 2011; 270: 377–87.

Sharpe LJ, Brown AJ. Controlling cholesterol synthesis beyond 3-hydroxy-3-methylglutaryl-CoA reductase (HMGCR). J Biol Chem 2013; 288: 18707–15.

Silvestrini M, Viticchi G, Falsetti L, Balucani C, Vernieri F, Cerqua R, et al. The role of carotid atherosclerosis in Alzheimer's disease progression. J Alzheimers Dis 2011; 25: 719–26.

Sperling RA, Aisen PS, Beckett LA, Bennett DA, Craft S, Fagan AM, et al. Toward defining the preclinical stages of Alzheimer's disease: recommendations from the National Institute on Aging-Alzheimer's Association workgroups on diagnostic guidelines for Alzheimer's disease. Alzheimers Dement 2011; 7: 280–92.

Sturchler-Pierrat C, Staufenbiel M. Pathogenic mechanisms of Alzheimer's disease analyzed in the APP23 transgenic mouse model. Ann N Y Acad Sci 2000; 920: 134–9.

Tabas I. Consequences of cellular cholesterol accumulation: basic concepts and physiological implications. J Clin Invest 2002; 110:905–11.

Thelen KM, Falkai P, Bayer TA, Lutjohann D. Cholesterol synthesis rate in human hippocampus declines with aging. Neurosci Lett 2006; 403: 15–19.

Thinakaran G, Koo EH. Amyloid precursor protein trafficking, processing, and function. J Biol Chem 2008; 283: 29615–19.

Vance JE. Dysregulation of cholesterol balance in the brain: contribution to neurodegenerative diseases. Dis Model Mech 2012; 5:746–55.

Vetrivel KS, Thinakaran G. Amyloidogenic processing of beta-amyloid precursor protein in intracellular compartments. Neurology 2006; 66: S69–73.

von Arnim CA, von Einem B, Weber P, Wagner M, Schwanzar D, Spoelgen R, et al. Impact of cholesterol level upon APP and BACE proximity and APP cleavage. Biochem Biophys Res Commun 2008; 370: 207–12.

Wendell CR, Waldstein SR, Ferrucci L, O'Brien RJ, Strait JB, Zonderman AB. Carotid atherosclerosis and prospective risk of dementia. Stroke 2012; 43: 3319-24.

Xie C, Lund EG, Turley SD, Russell DW, Dietschy JM. Quantitation of two pathways for cholesterol excretion from the brain in normal mice and mice with neurodegeneration. J Lipid Res 2003; 44: 1780–9.